Proceedings of the Thirty-third (2023) International Ocean and Polar Engineering Conference **www.isope.org**
Ottawa, Canada, June 19-23, 2023

ISBN 978-1-880653-80-7; ISSN 1098-6189

Robust SHM Systems Using Bayesian Model Updating

Jan-Hauke Bartels [a], Thomas Potthast [b], Masaru Kitahara [c], Steffen Marx [a], Michael Beer [b, d]
a) Institute of Concrete Structures, TU Dresden, Dresden, Germany
b) Institute for Risk and Reliability, Leibniz University Hannover, Hannover, Germany
c) Department of Civil Engineering, The University of Tokyo, Tokyo, Japan
d) Institute for Risk and Uncertainty, University of Liverpool, Liverpool, United Kingdom

ABSTRACT

Structural Health Monitoring (SHM) is becoming increasingly important for monitoring infrastructures. However, one of the main challenges is that the changes due to aging are small, not only for structures, but also for SHM systems. Hence, the question is how should we distinguish such changes due to aging from measurement uncertainty. In this study, laser triangulation sensors (LTSs) are tested and the uncertainty due to temperature effects is studied. Furthermore, time-dependent experiments are performed and the SHM system is calibrated over time through Bayesian Model Updating, considering its temperature dependence.

KEY WORDS: SHM; Bayesian Model Updating; temperature influence; laser triangulation sensor; measurement uncertainties; aging monitoring systems

INTRODUCTION

For condition monitoring of structures, Structural Health Monitoring (SHM) is becoming increasingly important, as it allows continuous condition assessment of the structure and usefully supplements on-site inspections (Farrar & Worden, 2007; Wedel & Marx, 2022). The aim of monitoring is to identify changes in the condition of the structure that can only be inadequately detected by the purely visual inspection (Worden et al., 2007), whereby the goal of monitoring can only be achieved by comparing at least two different states: the reference state with the current state (Worden & Tomlinson, 2019). For large infrastructures (e.g., wind turbines or bridges), however, the change in condition due to aging is very small (Klein et al., 2022). Typical measurements in structures are displacement measurements, since changes in the condition of the structure can be detected mainly by relative displacements of individual components (Bergmeister et al., 2015; Marx et al., 2015; Mischo et al., 2022). Laser measurements based on the triangulation principle enable a precise and robust measurement principle in practice, which detects the smallest displacements on the structure and enables contactless measurement (Bartels et al., 2023a; Löffler-Mang, 2012).

A general problem with monitoring systems, however, is that these systems age, just as structures do, and we suspect that the reliability of the monitoring system will decline over time. The question arises how aging of the measurement system can be considered in the data evaluation and how Bayesian Model Updating (BMU) enables a semi-automated data evaluation to give the interpreting engineer a tool that makes the data evaluation easier. This paper provides a contribution to this.
For this, the basic idea of BMU is explained first. Then, laboratory experiments are used to investigate the temperature and time dependence of the measurement system. Subsequently, it is shown how the time-dependent effects of the measurement system is reflected in the measurement data and how these effects can be taken into account in the condition assessment of structures. The semi-automatic data evaluation with BMU is described and potential improvements are discussed. The paper ends with a summary and an outlook.

BAYESIAN MODEL UPDATING METHOD

For engineering problems, mathematical models are typically used to simulate and evaluate the behavior of structures under load conditions. This virtual behavior corresponds only poorly to the real physical structure. To solve this problem, model updating techniques can be applied to update physical input parameters, e.g., material properties of a structure (Worden & Tomlinson, 2019). The physical parameters often cannot be measured directly. Therefore, a model update is required to derive these parameters so that the difference between the mathematical model and the real physical behavior of the system is minimized.
The physical behavior of a system is described by a function $M(x; \boldsymbol{\vartheta})$, where x defines the vector of unchangeable model parameters and $\boldsymbol{\vartheta}$ the vector of changeable model parameters to be updated. The mathematical relationship between the requested quantity $\boldsymbol{D}$ and the prediction model $\mathrm{M}(x; \boldsymbol{\vartheta})$ is defined by

$$\boldsymbol{D} = M(\boldsymbol{x}, \boldsymbol{\vartheta}) + \epsilon, \tag{1}$$

where ϵ describes the model or/and measurement error. The uncertainty

in the model parameters $\boldsymbol{\vartheta}$ can be accounted for using a probability density function (PDF). The problem in reality is that the best-fit joint PDF is not known, which links the model parameters $\boldsymbol{\vartheta}$ to the data $\boldsymbol{D}$. The advantage of BMU is that prior information about the model parameters $\boldsymbol{\vartheta}$ can be combined with the observed data $\boldsymbol{D}$ to infer the best-fit joint PDF. This leads to a posterior distribution of the model parameters $\boldsymbol{\vartheta}$ under the condition of the observations $\boldsymbol{D}$, using Bayes' theorem (Lye et al., 2021)

$$P(\boldsymbol{\vartheta}|\boldsymbol{D}) = \frac{P(\boldsymbol{D}|\boldsymbol{\vartheta}) \cdot P(\boldsymbol{\vartheta})}{P(\boldsymbol{D})}, \tag{2}$$

where $\boldsymbol{D}$ represents the observation vector, $P(\boldsymbol{\vartheta})$ the prior distribution, $P(\boldsymbol{D}|\boldsymbol{\vartheta})$ the likelihood function, $P(\boldsymbol{D})$ the evidence, and $P(\boldsymbol{\vartheta}|\boldsymbol{D})$ the posterior distribution. Since the analytical solution is usually not available for the posterior distribution $P(\boldsymbol{\vartheta}|\boldsymbol{D})$, Transitional Markov Chain Monte Carlo (TMCMC) sampler is used to sample from the posterior distribution. Basically, BMU uses actual data to reduce the uncertainty in a model to gain a better understanding of the relationship between model parameters and data. One method for performing BMU is TMCMC, a special form of the Markov Chain Monte Carlo (MCMC) algorithm that is useful for problems with fast transient transitions in the distribution. Unlike other MCMC methods that assume a steady state, TMCMC starts in a transient state and then transitions to the steady state, allowing for faster convergence of the chain. For more detailed information on the TMCMC algorithm, please refer to Ching and Chen (2007).

The accuracy of BMU with TMCMC is influenced by several factors, such as the quality and quantity of available data, the choice of model parameters, and the accuracy of the mathematical model. If the model does not describe the underlying physics or mechanisms with sufficient accuracy, the results may be unreliable. Therefore, it is important to use a model that describes the underlying physics or mechanisms with sufficient accuracy to achieve higher accuracy results. In the following sections, real measurement data in the form of distance measurements will be used to update a compensation model for the temperature effect on measurement systems using BMU. Therefore, the first step is to find a mathematical model that is as accurate as possible in order to minimize the uncertainties from the quality and quantity of the data as well as the uncertainties of the mathematical model.

EXPERIMENTAL SETUP AND TRANSFER FUNCTION

For the investigation of the temperature influence on laser measurements, a total of six Laser Triangulation Sensors (LTSs) within a measuring system are exposed to different temperature and air humidity levels within a climate chamber. The data is analyzed to determine whether and how the measurement signal changes. Initially, time-invariant investigations are carried out by examining the temperature dependence of the measuring system in short-term tests and using a temperature-dependent transfer function to compensate for the time-invariant systematic temperature influences.

In the subsequent time-variant investigations, the measurement system is exposed to different temperature and humidity over time to determine whether the temperature-dependent transfer function changes.

Sensors, Measurement System and Environmental Influences

The experimental setup is shown in Figure 1.

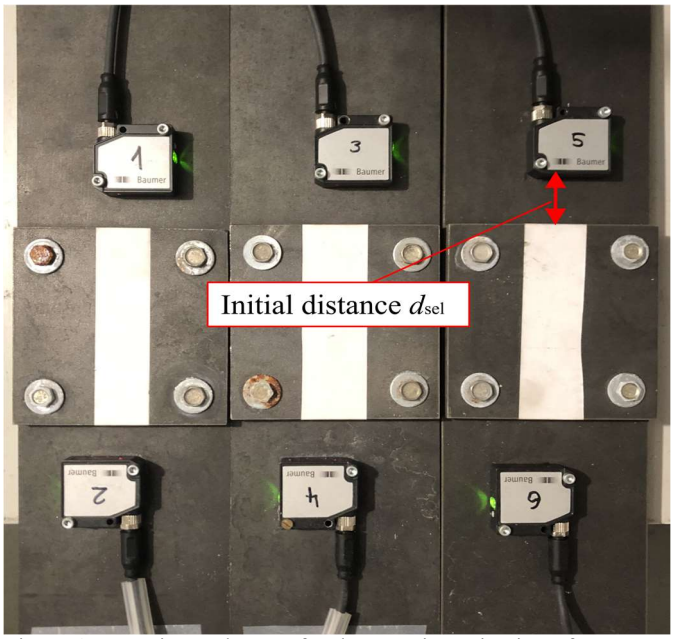

Figure 1. Experimental setup for the LTS investigation of temperature and time dependence.

The entire measuring system consists of LTS, cable and measuring amplifier. As can be seen in Figure 1, the LTS is fixed on a base plate with upstand and it measures the horizontal distance to the upstand. The special feature is, that the base plate and the upstand are made of the material Alloy 36, an iron-nickel alloy with a small coefficient of thermal expansion ($\alpha_{T,\text{Alloy36}} = 0.50 \cdot 10^{-6}$ 1/K). Compared to this material, construction steel ($\alpha_{T,\text{Steel}} = 13.00 \cdot 10^{-6}$ 1/K) has a coefficient of thermal expansion more than 20 times higher. With this design, it is possible to attribute changes in the measurement signal to the measurement system, since the influence of base plate strain due to temperature change is negligible (Bartels et al. 2023). LTSs with a measuring range of 10 mm are tested, which measure within the measuring distances 16 mm to 26 mm. To examine the entire measurement range of the LTS, three initial distances d_{sel} between the sensor and the upstand are selected ($d_{sel} \approx$ [17 mm; 21 mm; 25 mm]).

In the first step of analyzing only the temperature dependency, temperatures are varied between -10 °C and +50 °C in 10 K steps. The intended temperature curve can be seen in Figure 2.

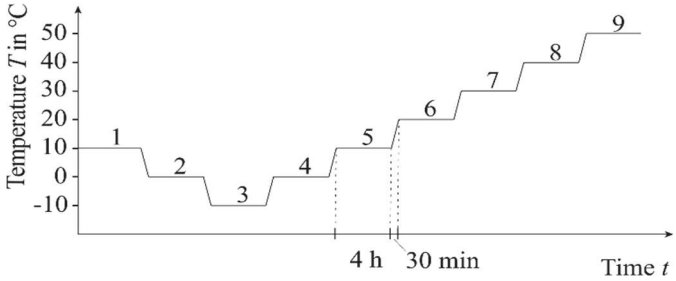

Figure 2. Intended temperature regulation for the investigation of temperature dependency of the SHM system.

This temperature curve covers the order of magnitude of temperatures that can typically occur on engineered structures. A temperature change of 10 K is chosen to cover a large temperature range in a reasonable amount of time. In addition, the temperature is held constant for 4 h and cooled or heated for 30 min with a temperature gradient of 0.33 K/min to allow the experimental setup to follow the temperature gradient. To investigate possible hysteresis effects, the temperature gradient is started at 10 °C, then reduced to 0 °C and -10 °C, and then increased again to 0 °C and 10 °C up to 50 °C in 10 K steps. This is to investigate whether the behavior of the measurement system depends not only on the current temperature but also on its previous states. Previous investigations have shown that there is no influence of hysteresis on the behavior of the measurement system (Bartels, 2022).

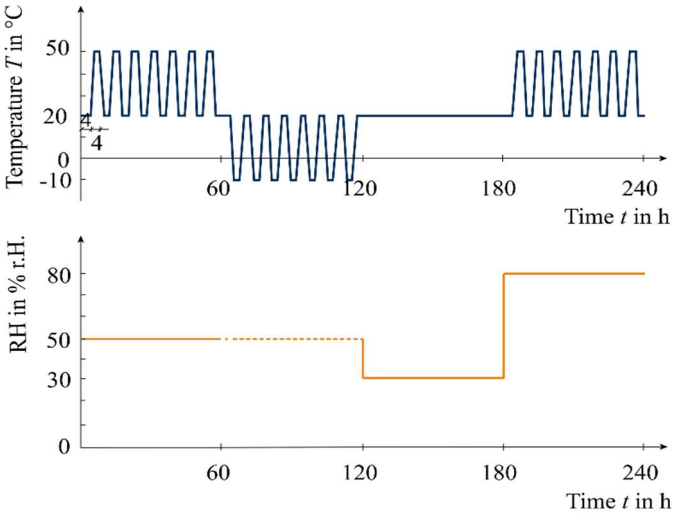

Figure 3. Intended temperature and humidity regulation for the investigation of time dependency of the SHM system

In the second step of analyzing the time dependency, the SHM system is subjected to a modified temperature and humidity curve (see Figure 3) using the same experimental setup shown in Figure 1.
Following the temperature curve in Figure 3, the sequence between constant temperature and temperature change is chosen to be 4.50 h. The climate cycle consists of several phases, which are supposed to represent the natural conditions of the day-night cycle, but with an accelerated sequence by a factor of 5.33. During a phase, the temperature is cyclically varied between a maximum and a minimum temperature. To investigate long-term stability, a sequence of four phases was defined following previous studies (Herrmann et al., 2015) and the standards for environmental testing of electrotechnical products (Beuth Verlag GmbH, 2007a, 2007b). The four phases are repeated continuously over the entire test period, with phase 1 starting after 10 d in each case. The climate cycle has been shown in previous research to be suitable for accelerated temperature and humidity exposure (Herrmann et al., 2015). Each phase begins with a temperature of 20 °C and the accelerated temperature progression of five temperature cycles per day is slow enough to keep the humidity as constant as possible and allow the samples to follow the temperature gradient.

Temperature Dependent Transfer Function

By varying the temperature, a reproducible test of the SHM system with respect to the temperature dependency is possible. Keeping the temperature constant for 4 h has two objectives: on the one hand, the temperature inertia of the experimental setup is overcome, so that the temperature can be assumed for the whole system, consisting of SHM system and base plate. On the other hand, a representative amount of data can be generated over this period. With a sampling rate of 1 Hz, 14,400 measured values are generated over 4 h. Only the constant temperature and measurement distance ranges are cut out of the raw data signal, so that there are less than 14,400 measured data points used for the analysis.

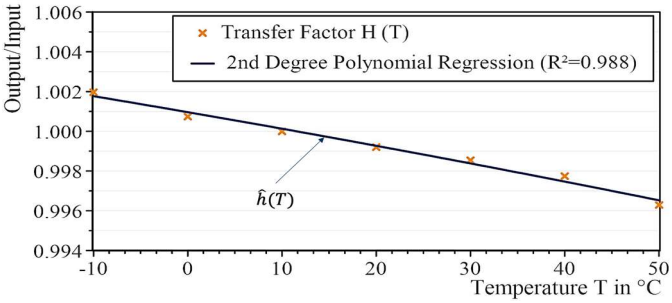

Figure 4. Temperature dependent transfer function for one LTS

This procedure is carried out for all temperature levels resulting in a total of seven expected values from -10 °C to +50 °C. The values are related to the measured distance at 10 °C (reference value). This quotient between the measurement distance at a given temperature and the measurement distance at 10 °C is referred to as the transfer factor $H(T)$. The individual transfer factors are approximated by a 2nd degree regression polynomial to the so-called temperature-dependent transfer function $\hat{h}(T)$, see Figure 4. The detailed description of the procedure for calculating the temperature dependent transfer function is given in (Bartels et al., 2023a).

Time Dependence of the Transfer Function

The temperature and humidity curve, shown in Figure 3, can be divided into four phases, with each phase starting and ending at a temperature of 20 °C. This has the advantage that the output signal (at 20 °C) after each aging phase can be compared with the input signal (also at 20 °C) at the beginning of the experiment. In order to be able to record the time variance of the transfer function, the test for determining the temperature-dependent transfer function according to the aforementioned subsection is carried out after each 240-hour aging test and compared with the transfer function from Figure 4. The result is shown in Figure 5.

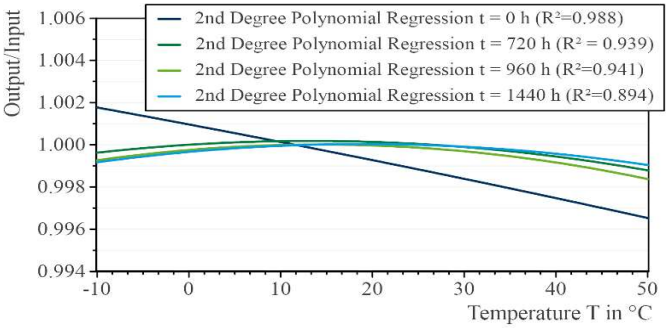

Figure 5. Investigation of the time variance of the temperature-dependent transfer function

In order to also control the humidity, the experimental setup had to be installed in another climate chamber in which both the temperature and

the humidity can be varied, as shown in Figure 3. At time $t = 0$ h, the experimental setup is in the "old" climate chamber, at time $t = 720$ h, the experimental setup is in the "new" climate chamber. Figure 5 shows that the temperature-dependent transfer function changes when the measurement system is disassembled and reassembled in a different location. After the measurement system is installed in the new climate chamber, the temperature-dependent transfer function hardly changes, so the time points 720 h, 960 h, and 1440 h were chosen to consider the time dependence of the measurement system. These values represent the time points after each aging cycle of 240 h. In practical applications for SHM systems, the transfer function must first be determined at the application site to compensate for the systematic temperature effect. It is not possible to determine the function in the laboratory and use it for on-site measurements. The fact that the transfer function hardly changes over time once the measurement system is no longer moved helps us in a later section when applying BMU, as we do not have to consider a significant change in the functional structure, since it remains a 2nd degree polynomial. Since this temperature-dependent transfer function shows the relative change in measured value to the reference value at $T = 10$ °C, time variances can be derived out of Figure 5. If we look at the median at each time with the temperature of $T = 20$ °C, the time variance becomes visible over the period under consideration. The result for three LTSs (blue color) is shown in Figure 6.

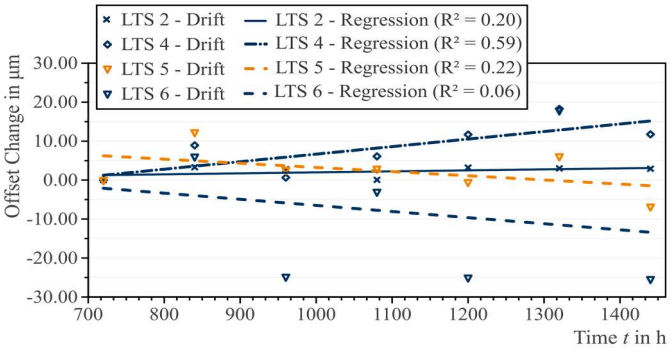

Figure 6. Median values of the laser displacement measurement over time at 20 °C and 50 % r.H.

We determined the arithmetic mean at $T = 20$ °C after 120 h in each case, at 20 °C and 50 % r.H., so that compensation due to systematic environmental influences is not necessary to compare the values with each other. Since the SHM system is no longer moved at time t = 720 h, the period between 720 h and 1440 h is shown in Figure 6.

Over time, the median value changes in all three cases. A measured value drift is visible. Such a measured value drift is often not uncommon in practice. If drift occurs in practice, it can be corrected by recalibrating the SHM system. In these laboratory experiments, LTSs 2, 4, and 6 are evaluated and not recalibrated to assess the change in measurement signal over time. The three sensors are chosen because they are installed on the specimens with initial distances of 17, 21, and 25 mm, which covers the entire measurement range of the LTSs used. In addition, all three sensors are installed on the same side of the specimen so that the results can be compared. If we were to compare the sensors on the opposite side with these sensors, non-detectable systematic influences such as light sources or influences from the air humidity circulation within the climate chamber could falsify the results.

The measured value drift is visible in all three sensors, whereby the smallest measured value drift is observed for LTS 2 with an initial distance of 17 mm, and the largest measured value drift occurs for LTS 6 with an initial distance of 25 mm. Furthermore, it can be seen that the slope of the regression line is positive for LTS 2 and LTS 4, while it is negative for LTS 6. In this regard, it should be noted that the change in measured value after the aging phases is very large for LTS 6 compared to LTS 2 and LTS 4, although identical environmental conditions are present for all three sensors and at all measurement time steps. In the evaluation of the data, this observation is reflected in the coefficient R^2, which is comparatively small for LTS 6 with $R^2 = 0.06$ and thus only inadequately describes the measured value drift over time. One reason for the unsteady change in the measurement signal over time could be the temperature-dependent change in sensor component position within the sensor housing, which can occur with LTS 6 due to quality differences in sensor manufacture, or which is more pronounced than with smaller initial distances due to the larger initial distance of 25 mm. Against the larger initial distance argues that the measured values of the comparison sensor LTS 5 in Figure 6 (orange color) do not scatter as much as LTS 6. Another reason could also be an aging of the sensor for the change in measured values, which is visible faster in LTS 6 than in LTSs 2 and 4. This will be investigated in the next step.

With these results we speak in all three cases of a time-variant SHM system with reversible signal properties. Nevertheless, time variance with reversible measuring signal properties should not be mixed up with aging. We speak of aging when the SHM system is time variant and has irreversible signal system properties. The phenomenon of measurement drift is reversible with recalibration. The increase in measurement uncertainty, on the other hand, is irreversible. In the next step we will evaluate the change of the scatter of the measurement signal for the three sensors over time.

Typically, two times the standard deviation (2 x SD) is specified in metrology as measurement uncertainty, as this allows a degree of reliability of at least 95 % for the range of measured values assuming a normal distribution. In the conducted tests the 2.5 % and the 97.5 % quantiles are calculated. In future analyses, the distribution type should be analyzed in more detail. With the help of the definition of the distribution type, more detailed information about the measurement data is possible, e.g., the interpretation of the measurement data as measurement noise. In this paper, the difference between the quantiles (95 % confidence interval) is calculated and shown for the different time steps of aging in Figure 7 for three different LTSs.

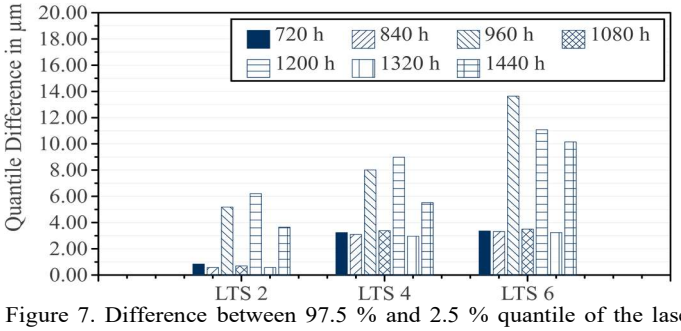

Figure 7. Difference between 97.5 % and 2.5 % quantile of the laser displacement measurement over time at 20 °C and 50 % r.H.

First of all, it is noticeable that the scattering tends to be lower at initial distances of 17 mm (LTS 2) than at 21 mm (LTS 4) or 25 mm (LTS 6). This is due to the fact that at greater distances a diffuse laser beam is produced rather than an ideal laser spot on the object surface. This scattering is also transferred to the position-sensitive detector so that the measurement with LTS becomes less accurate with increasing distance to the object surface (Bartels et al., 2023a). At $t = 720$ h the difference is approximately 1.00 µm for LTS 2 and 3.00 µm for LTS 4 and 6. If aging had taken place, the scattering would successively increase over the

considered time points. This cannot be observed for all three tested LTSs. At time points t = 840 h, 1,080 h, and 1,320 h, the scatter for all three LTSs is the same value as at time point t = 720 h. Therefore, so far, no aging of the measurement system can be assumed in the considered period. Nevertheless, at the times t = 960 h, 1,200 h and 1,440 h significant increases of the scatter are noticeable. It is not possible to say exactly where this increase in scatter comes from. However, it is noticeable that the scatter increases at the same times for all tested sensors. One reason could be the external power supply of the sensors, which can contaminate the output signal of the LTS when the power supply is highly loaded by other connected electrical devices. This assumption will be further investigated in future tests.

ENGINEERING INTERPRETATION AND BAYESIAN MODEL UPDATING

In this chapter, we will explain how we can use the previously achieved findings in SHM practice. For this, the transfer functions at the different points in time are to be considered first, with which a statement about the reliability of the measurement signal should be made. In addition, the application of BMU in SHM will be described.

Engineering Interpretation of Theoretical Findings

In Figure 5 it looks like the temperature dependent transfer function of the tested LTS barely changes. With the drift of the measured values shown in Figure 6, a time variance is inferred, while the almost constant quantile differences shows that no aging of the SHM system has yet occurred. To make the results from Figs.Figure 5-7 applicable to a practicing engineer, the temperature dependent transfer function is calculated at different points in time t = {720 h; 960 h: 1,440 h}. Figure 8 shows three bundles of a set of curves at different times for LTS 4. A bundle of one transfer function is represented by the median values, the 2.5 %, and the 97.5 % quantile at the specific time points. The reference value is at t = 720 h and 10 °C. It can be seen that the transfer function barely changes at low temperatures (e.g., -10 °C and 0 °C), whereas a widening of the function set can be seen at higher temperatures. This means that the polynomial bundles show an expansion with respect to each other for the three-time points considered, making the measurement less reliable. The reason for that is the aforementioned measurement drift. If we look at the quantile differences, it becomes clear that these do not change. This confirms the observations of no aging phenomena from Figure 7.

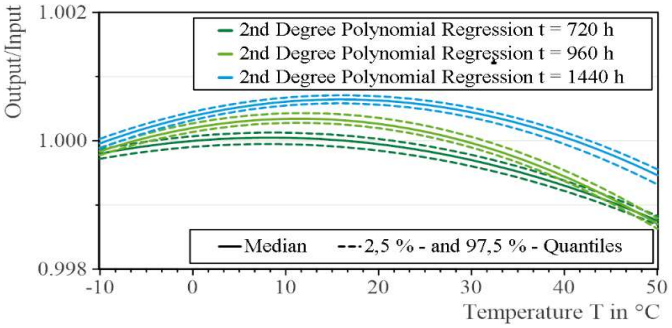

Figure 8. Transfer functions at different times with 2.5 % and 97.5 % quantiles

Using these transfer functions, both a temperature compensation of the raw data signal and an evaluation of a change in structural condition can be performed. The latter is shown in the following example.

To have an order of magnitude of a typical distance measurement on real infrastructures, research articles were reviewed that describe SHM applications on real structures with laser distance measurements. For instance, for rigid railroad arch bridges, the deflection at the center of the arch is less than 0.30 mm (300 µm) (Bergmeister et al., 2015). Deflections of 15 mm (15,000 µm) are not unusual in monitoring systems used as a tool for bridge monitoring during soil compaction work (Marx & Wenner, 2015). In contrast, magnitudes smaller than 0.05 mm (50 µm) have been reported for monitoring relative tower segment displacements during wind turbine tensioning operations (Klein et al., 2022). Although the choice of the LTS depends significantly on the measurement task and the possible measurement range, the latter specification (50 µm) is defined as the minimum requirements for the measurement accuracy of the LTS for the example. A reference value in the middle of the measuring range of the LTS is assumed, so that the transmission factor is calculated to be 21.05 / 21.00 = 1.002. For example, at the time of t = 1440 h and a temperature of 20 °C, such a condition change would still be detectable, since this value is outside the range of the curves. However, as the SHM system ages, the transfer function could drift further. The quantile difference could also increase with time, so that at a certain point in time this condition change could not be detected on the structure. However, this requires calibration of the SHM system at certain intervals or replacement of certain measurement chain components. Another option is to calibrate the transfer function with the BMU. This has the advantage that the SHM system itself can be monitored at arbitrary times in quasi-real time by updating the mathematical model. This procedure will be shown in the next chapter.

Application of Bayesian Model Updating

For this, the transfer function from the manual approximation of the temperature dependent transfer function from time point t = 720 h to time point t = 960 h and from t = 960 h to t = 1,440 h is compared with the one generated by BMU to determine the error made in the semi-automation of the updating. To perform BMU, only two things need to be done. First, the mathematical model that is to be updated has to be stored as a reference model. Second, the raw measurement data of the laser distance measurement clustered by temperature have to be imported. In this chapter, the manual approximation (2nd degree regression polynomial) is compared with the BMU and the error is calculated.

For this, the mathematical reference model of the transfer function is important, which includes the parameters ϑ_i to be updated. With the equation (3)

$$\hat{h}(T, \vartheta_i) = 1.0 \cdot \vartheta_1 + 1.2 \cdot 10^{-5} \cdot T \cdot \vartheta_2 - 7.4 \cdot 10^{-7} \cdot T^2 \cdot \vartheta_3 \qquad (3)$$

the transfer function for updating is defined at time t = 720 h, where T is the temperature. In the manual approximation of the transfer function at time t = 960 h, the parameters of the 2nd degree regression polynomial are determined so that they can be compared with the parameters of the transfer function at time t = 720 h. The quotient of the respective parameters results is the fitting factor ϑ_i.

For the validation of BMU, the change of the transfer function is considered once between the time points t = 720 h to t = 960 h and between t = 960 h to t = 1,440 h. The results are listed in Table 1.

Table 1. Comparison of manual approximation and BMU (TMCMC)

		ϑ_1	ϑ_2	ϑ_3
	Manual	1.00020	2.03724	1.47984
t = 720 h to 960 h	BMU	1.00051	2.09413	1.51431
	Error	0.010 %	2.793 %	2.329 %
	Manual	1.00034	0.60755	0.68738
t = 960 h to 1440 h	BMU	1.00025	0.65980	0.68000
	Error	0.008 %	8.600 %	1.074 %

It becomes clear that the error between manual approximation and BMU is small. In both cases, the change of the transfer function over time is relatively small, although the period is 240 h in the first BMU process and 480 h in the second one. In both cases, the deviation is less than 10 %. Nevertheless, the fitting factors in the BMU process are determined with some uncertainty, since an expected value is calculated on the basis of a large number of samples, which is computed with a standard deviation. In future experiments, it will be investigated how large the standard deviation of the individual parameters can be so that the smallest changes in the transfer functions can be reliably determined and are not lost in the standard deviation of the fitting factors. Moreover, the BMU was performed several times for both cases to check its reproducibility. In some cases, considerable deviations occurred since the parameters ϑ_i to be updated do not converge. This problem must be investigated and minimized in future calculations as best as possible to ensure practical use without errors. Therefore, the application of the BMU in SHM practice must be done with great care and caution.

CONCLUSION AND OUTLOOK

In this paper, a SHM system typically used in practice was tested under laboratory conditions for its temperature dependence and its time dependence. A method for the temperature compensation of laser measurements was presented. Then, the time dependent changes as well as the aging of a SHM system was investigated. Based on this, the application example of the theoretical findings was shown by means of a fictional example and the idea of BMU was implemented in the SHM process, with which an update of transfer functions can run semi automatically over time. Several findings were made in this paper, which can be described as follows:

- Laser displacement measurements are temperature and time dependent. The temperature dependence represents a systematic measurement error that must be compensated for using the generated temperature dependent transfer function. We were able to detect the time dependence over the period considered because a drift of the median was observed. Aging shows up in the form of an increase in the quantile difference. The latter could not be identified so far.
- It is shown that the generation of the temperature-dependent transfer function must first be applied to the structure to be monitored in order to perform reliable temperature compensation. After the SHM system is built into a different climate chamber, different results are obtained for the same LTS.
- So far, the time variance of the SHM system is so low over the time period considered that even a supposedly minor change in the condition of the structure can be reliably detected.
- The application of a BMU shows promising results for the semi-automated fitting of the mathematical model of the transfer function of a SHM system over time. Thus, this procedure providing the interpreting engineer with a helpful tool for semi-automated temperature compensation in the presence of time-variant behavior of the measurement system.

In future investigations, further aging tests will be carried out to confirm the assumption of increasing quantile differences and thus be able to show the effect of aging. In addition, we will analyze the raw measurement data in more detail by specifying the distribution of the measurement data. This allows us to make more informative statements about the measurement data, such as specifying an arithmetic mean instead of the median, or specifying the standard deviation instead of the quantile difference. These two parameters are typically given in metrology. Further, the BMU algorithm will be improved to make the update of the mathematical model more reliable than it is now. In addition, the concept presented here will be validated on real structures such as wind turbines and written up in future scientific papers. Nevertheless, the results show a promising approach for reliable SHM use. With this method, marginal change in the measurement system and at the structure can be reliably captured even over several years.

ACKNOWLEDGEMENTS

This research was funded by the German Research Foundation (DFG), as part of the Collaborative Research Centre 1463 (SFB 1463) "Integrated Design and Operation Methodology for Offshore Megastructures" (subproject C01, project number 434502799).

REFERENCES

Bartels, J.-H. (2022). Robuste, lebensdauerumfassende Monitoringkonzepte für Offshore-Windenergieanlagen. In *Beiträge zum 61. Forschungskolloquium mit 9. Jahrestagung des DAfStb* (pp. 57–62). TU Dresden. https://doi.org/10.25368/2022.378

Bartels, J.-H., Gebauer, D., & Marx, S. (2023). „Einflüsse auf die Messunsicherheit von SHM-Systemen und deren Kompensation am Beispiel von Laser-Distanzmessungen," *Bautechnik.* Advance online publication. https://doi.org/10.1002/bate.202200102

Bartels, J.-H., Potthast, T., Kitahara, M., Marx, S., & Beer, M. (2023a). Influences on Measurement Uncertainty in SHM Systems and their Compensation Using the Example of Laser Distance Measurement. *Structural Health Monitoring SAGE*, *Under Review*.

Bergmeister, K., Mark, P., Österreicher, M., Sanio, D., Heek, P., Krawtschuk, A., & Strauss A. (2015). „Innovative Monitoringstrategien für Bestandsbauwerke," *Beton-Kalender 2015* 315–458. https://doi.org/10.1002/9783433603406.ch7

Beuth Verlag GmbH (2007a). *Environmental testing - Part 2-1: Tests - Test A: Cold (IEC 60068-2-1:2007); German version EN 60068-2-1:2007*. Beuth Verlag GmbH: Beuth Verlag GmbH.

Beuth Verlag GmbH (2007b). *Environmental testing - Part 2-2: Tests - Test B: Dry heat (IEC 60068-2-2:2007); German version EN 60068-2-2:2007*. Beuth Verlag GmbH: Beuth Verlag GmbH.

Ching, J., & Chen, Y.-C. (2007). "Transitional Markov chain Monte Carlo method for Bayesian model updating, model class selection, and model averaging," *Journal of Engineering Mechanics*. (7), 816–832.

Farrar, C. R., & Worden, K. (2007). "An introduction to structural health monitoring," *Phil. Trans. R. Soc. A.*, *365*, 303–315. https://doi.org/10.1098/rsta.2006.1928

Herrmann, R., Stockmann, M., & Marx, S. (2015). Untersuchungsstrategie zur Bewertung der Langzeitstabilität von

Dehnungsmessstreifen. *Bautechnik*, *92*(7), 451–460. https://doi.org/10.1002/bate.201500018

Klein, F., Fürll, F., Betz, T., & Marx, S. (2022). "Experimental study on the joint bearing behavior of segmented tower structures subjected to normal and bending shear loads," *Structural Concrete*, *23*, 1370–1384. https://doi.org/10.1002/suco.202100710

Löffler-Mang, M. (2012). „Triangulation," In *Optische Sensorik* 172–177. Vieweg + Teubner Verlag. https://doi.org/10.1007/978-3-8348-8308-7_20

Lye, A., Cicirello, A., & Patelli, E. (2021). "Sampling methods for solving Bayesian model updating problems: A tutorial," *Mechanical Systems and Signal Processing*, *159*, 107760.

Marx, S., Krontal, L., & Tamms, K. (2015). „Monitoring von Brückenbauwerken als Werkzeug der Bauüberwachung," *Bautechnik*, *92*, 123–133. https://doi.org/10.1002/bate.201500002

Marx, S., & Wenner, M. (2015). „Structural Health Monitoring (SHM) an der Scherkondetalbrücke: eine semi-integrale Eisenbahn-Betonbrücke," *Beton- Und Stahlbetonbau*, *110*, 2–8. https://doi.org/10.1002/best.201500501

Mischo, H., Sanio, D., Strohbusch, J., Seisenberger, J., Schartner, M., Kargus, D., & Mündecke, E. (2022). „Monitoring für Ingenieurbauwerke – Ein Anwenderbericht aus der Sicht eines Ingenieurbüros," *Bautechnik*, *99*, 556–564. https://doi.org/10.1002/bate.202200048

Wedel, F., & Marx, S. (2022). "Application of Machine Learning Methods on Real Bridge Monitoring Data," *Engineering Structures*, *250*, 113365. https://doi.org/10.1016/j.engstruct.2021.113365

Worden, K., Farrar, C. R., Manson, G., & Park, G. (2007). "The fundamental axioms of structural health monitoring," *Proceedings of the Royal Society a: Mathematical, Physical and Engineering Sciences*, *463*, 1639–1664. https://doi.org/10.1098/rspa.2007.1834

Worden, K., & Tomlinson, G. R. (2019). *Nonlinearity in structural dynamics: detection, identification and modelling,* CRC Press.